WATER RESOURCES RESEARCH, VOL. 50, 681–686, doi:10.1002/2013WR014619, 2014

A comparison between simulation and experiment for hysteretic phenomena during two-phase immiscible displacement

F. Doster[1,2] and R. Hilfer[3,4]

Received 21 August 2013; revised 12 December 2013; accepted 16 December 2013; published 28 January 2014.

[1] The paper compares a theory for immiscible displacement based on distinguishing percolating and nonpercolating fluid parts with experimental observations from multistep outflow experiments. The theory was published in 2006 in *Physica A*, volume 371, pages 209–225; the experiments were published in 1991 in *Water Resources Research*, volume 27, pages 2113. The present paper focuses on hysteretic phenomena resulting from repeated cycling between drainage and imbibition processes in multistep pressure experiments. Taking into account, the hydraulic differences between percolating and nonpercolating fluid parts provides a physical basis to predict quantitatively the hysteretic phenomena observed in the experiment. While standard hysteretic extensions of the traditional theory are nonlocal in time the theory used in this paper is local in time. Instead of storing the pressure and saturation history, it requires only the current state of the system to reach the same quantitative agreement.

Citation: Doster, F., and R. Hilfer (2014), A comparison between simulation and experiment for hysteretic phenomena during two-phase immiscible displacement, *Water Resour. Res.*, *50*, 681–686, doi:10.1002/2013WR014619.

1. Introduction

[2] A quantitative prediction of fluid saturation profiles during immiscible displacement remains a fundamental open problem in the physics of porous media. Despite its well-known limitations regarding hysteresis and trapping phenomena, the traditional approach [*Buckingham*, 1907; *Richards*, 1931; *Muskat and Meres*, 1936; *Wyckoff and Botset*, 1936] has remained the most popular mathematical model for more than 70 years in applications such as reservoir engineering [*Lake*, 1989] or groundwater hydrology [*Bear*, 1972].

[3] Many authors have emphasized the importance of hysteresis between drainage and imbibition [*Wei and Dewoolkar*, 2006; *Gerhard and Kueper*, 2003; *Parker*, 1989; *Mualem*, 1973]. Ad hoc extensions of the existing two-phase flow model [*Parker*, 1989; *Stauffer*, 1978; *Mualem*, 1974; *Land*, 1968] yield reasonable agreement with laboratory measurements. However, the physical foundations for such hysteresis models are not clear.

[4] A recent macroscopic theory of capillarity in porous media [*Hilfer*, 2006a] proposes to take into account the different hydrodynamic properties of percolating (= connected) and nonpercolating (= not connected) fluid parts. This provides the physical basis for hysteresis in our approach. In the residual decoupling limit, the traditional constitutive relations between relative permeability and saturation as well as between capillary pressure and saturation are recovered including hysteresis [*Hilfer*, 2006a, 2006b]. Approximate analytical results for a quasi-static displacement have been calculated in *Hilfer* [2006c]. In *Hilfer and Doster* [2009] and *Doster et al*. [2010], numerical solutions were calculated for experiments with a closed homogeneous column in gravity. Further, analytic and quasi-analytic solutions for the theory were developed in *Doster and Hilfer* [2011], *Doster et al*. [2012], and *Hönig et al*. [2013]. However, an explicit comparison with experimental data is pending.

[5] The objective of this paper is to close this gap. We show that the theory is able to model a laboratory experiment [*Lenhard et al*., 1991] with a porous column that shows hysteretic behavior.

[6] The paper is structured as followed. First, we illustrate the experimental setup [*Lenhard et al*., 1991] that has been used to illustrate hysteretic phenomena in fluid distributions in porous media flow. Section 3 briefly presents the theory of percolating and nonpercolating phases and its mathematical formulation for incompressible immiscible two-phase flow. In section 4, we discuss the numerical representation of the experiment and its implementation. The results are presented and discussed in section 5. The paper closes with concluding remarks.

2. Experimental Setup

[7] The experimental setup of *Lenhard et al*. [1991] consists of a vertical cylindrical, 72 cm long column, whose side walls are impermeable, filled with a homogeneous, isotropic and incompressible porous medium, an unconsolidated sandy material comprising approximately 97.5, 0.8 and 1.7% sand, silt, and clay-sized particles, respectively. The two fluids considered here are water and air and water

[1]Department of Civil and Environmental Engineering, Princeton University, Princeton, New Jersey, USA.
[2]Department of Mathematics, Bergen University, Bergen, Norway.
[3]Institut für Computerphysik, Universität Stuttgart, Stuttgart, Germany.
[4]Institut für Physik, Universität Mainz, Mainz, Germany.

Corresponding author: F. Doster, Department of Civil and Environmental Engineering, Princeton University, Princeton, NJ 08544, USA. (flodoster@gmail.com)

0043-1397/14/10.1002/2013WR014619

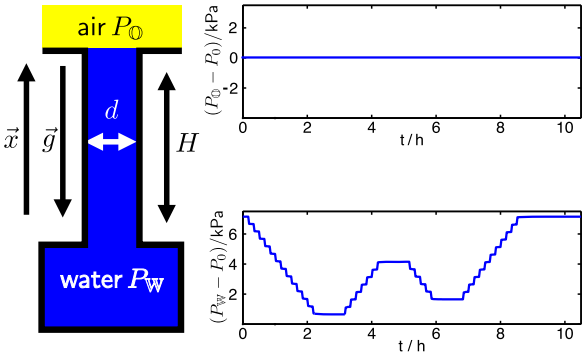

Figure 1. Conceptual picture of the experimental setup and the pressure protocols in the upper and lower reservoir versus time.

is the wetting fluid. The top of the column is connected to the atmosphere so that only air can enter the top of the column. The bottom of the column is connected to a water tank and only water can enter from the bottom. The pressure in the tank is adjustable. Initially, the porous column is completely water saturated and the pressure $P_{\mathbb{W}}$ in the water tank is chosen such that it compensates the water column $P_{\mathbb{W}}(t=0)=72$ cm $H_2O(=7.06\,\text{kPa})$. Hence, the capillary fringe is located at the top of the column. The pressures in this section are given in centimeters column of water because this translates one to one to the position of the water table in the column. In section 5, SI units are used. Figure 1 gives a conceptual picture of the experiment. The column is drained by lowering the pressure in the reservoir by $\Delta P=5$ cm H_2O every $\Delta t=10$ min 13 times until the water pressure reaches $P_{\mathbb{W}}=7$ cm H_2O. After a relaxation period of $\Delta t=50$ min, the water pressure is raised again in seven steps by $\Delta P=5$ cm H_2O every $\Delta t=10$ min and the column is imbibed again. After $\Delta t=50$ min, the water pressure is again lowered by $\Delta P=5$ cm H_2O every $\Delta t=10$ min for five times and the column is drained again. Finally, $\Delta t=50$ min later, the water pressure is raised again by $\Delta P=5$ cm H_2O steps every $\Delta t=10$ min until it reaches its initial value $P_{\mathbb{W}}(t>8\text{h})=72$ cm H_2O. However, the original water content in the column is not recovered because a fraction of air remains trapped in the medium [*Gerhard and Kueper*, 2003].

[8] In the laboratory, water saturation and water pressure have been measured at height $x=0.4$ m, $x=0.5$ m, $x=0.6$ m, and $x=0.7$ m from the bottom of the column. It may safely be assumed that the air pressure is essentially hydrostatic and atmospheric for two reasons: First, because of the high viscosity and density contrast ($\mu_{\mathbb{W}}=0.001$ kg m^{-1}s^{-1}, $\mu_{\mathbb{O}}=18\times10^{-6}$ kg m^{-1}s^{-1}, and $\varrho_{\mathbb{W}}=1000$ kg m^{-3}, $\varrho_{\mathbb{O}}=1.2$ kg m^{-3}) and second, because the column is short. It is, therefore, concluded that the measurement of water saturation and water pressure suffices to determine the capillary pressure-saturation relationship.

3. Definition of the Model

[9] In this section, a brief summary of the mathematical model is given. The following equations are based on volume, mass, and momentum balance equations analogous to the foundations of the traditional theory (see e.g., *Hilfer* [2006b] for a succinct but detailed parallel development). It is assumed that both fluids are incompressible and immiscible and that the lateral dimensions of the column are small with respect to the capillary fringe. Hence, a one-dimensional description is an appropriate approximation. The mass balances for the four fluid phases (percolating water is identified by the index 1, nonpercolating water by 2, percolating oil by 3, and nonpercolating oil by 4) read as

$$\varrho_{\mathbb{W}}\phi\frac{\partial S_1}{\partial t}+\varrho_{\mathbb{W}}\frac{\partial q_1}{\partial x}=M_1, \tag{1a}$$

$$\varrho_{\mathbb{W}}\phi\frac{\partial S_2}{\partial t}+\varrho_{\mathbb{W}}\frac{\partial q_2}{\partial x}=M_2=-M_1, \tag{1b}$$

$$\varrho_{\mathbb{O}}\phi\frac{\partial S_3}{\partial t}+\varrho_{\mathbb{O}}\frac{\partial q_3}{\partial x}=M_3, \tag{1c}$$

$$\varrho_{\mathbb{O}}\phi\frac{\partial S_4}{\partial t}+\varrho_{\mathbb{O}}\frac{\partial q_4}{\partial x}=M_4=-M_3, \tag{1d}$$

where t denotes time, x denotes position or height along the column, ϕ denotes porosity, $\varrho_{\mathbb{W}}, \varrho_{\mathbb{O}}$ denote the density of water, respectively, air, S_i is the saturation, q_i is the volume flux, and M_i is the mass exchange term of the phase i. The mass exchange term accounts for the fact that percolating and nonpercolating phases of the same fluid exchange mass by breakup and coalescence. The mass exchange terms take the form

$$M_1=\eta_2\phi\varrho_{\mathbb{W}}\left(\frac{S_2-S_2^*}{S_{\mathbb{W}}^*-S_{\mathbb{W}}}\right)\frac{\partial S_{\mathbb{W}}}{\partial t}, \tag{2a}$$

$$M_3=\eta_4\phi\varrho_{\mathbb{O}}\left(\frac{S_4-S_4^*}{S_{\mathbb{W}}^*-S_{\mathbb{W}}}\right)\frac{\partial S_{\mathbb{W}}}{\partial t} \tag{2b}$$

with the parameter functions

$$\begin{aligned}S_{\mathbb{W}}^*=&(1-\min(S_{\mathbb{O}\text{im}},(1-\epsilon_{\text{M}})S_{\mathbb{O}}))\Theta(\partial_t S_{\mathbb{W}})\\&+\min(S_{\mathbb{W}\text{dr}},(1-\epsilon_{\text{M}})S_{\mathbb{W}})[1-\Theta(\partial_t S_{\mathbb{W}})],\end{aligned} \tag{3a}$$

$$S_2^*=\min(S_{\mathbb{W}\text{dr}},(1-\epsilon_{\text{M}})S_{\mathbb{W}})[1-\Theta(\partial_t S_{\mathbb{W}})], \tag{3b}$$

$$S_4^*=\min(S_{\mathbb{O}\text{im}},(1-\epsilon_{\text{M}})S_{\mathbb{O}})[1-\Theta(\partial_t S_{\mathbb{O}})], \tag{3c}$$

where the parameter $S_{\mathbb{O}\text{im}}$ is a limiting saturation for the nonpercolating air, $S_{\mathbb{W}\text{dr}}$ is a limiting saturation for nonpercolating water, and $\Theta(\cdot)$ denotes the Heaviside step function. Water saturation is given by $S_{\mathbb{W}}=S_1+S_2$ and the air saturation by $S_{\mathbb{O}}=S_3+S_4$. The parameter $\epsilon_{\text{M}}\approx 0$ is a mathematical regularization parameter. It allows to simulate also primary processes. The volume fluxes of the phases take the form

$$\begin{pmatrix}q_1\\q_2\\q_3\\q_4\end{pmatrix}=\Lambda\begin{pmatrix}-\partial_x P_1-\varrho_{\mathbb{W}}g\\-\partial_x(P_3-\gamma P_2^* S_2^{\gamma-1})-\varrho_{\mathbb{W}}g+P_{\text{a}}\partial_x S_1^{-\alpha}\\-\partial_x P_3-\varrho_{\mathbb{O}}g\\-\partial_x(P_1-\delta P_4^* S_4^{\delta-1})-\varrho_{\mathbb{O}}g+P_{\text{b}}\partial_x S_3^{-\beta}\end{pmatrix}, \tag{4}$$

where P_1, P_3 denote the averaged pressures of the percolating phases, g is the gravity acceleration, and $\alpha, \beta, \gamma, \delta, P_{\text{a}}$,

Table 1. List of Parameters With Units and Their Numerical Values Used for Simulating the Experiment[a]

Parameters		Units	Values	
ϕ			0.36	
ϵ_M			0.01	
$\mathbb{W}$	$\mathbb{O}$		$\mathbb{W}$	$\mathbb{O}$
$\varrho_{\mathbb{W}}$	$\varrho_{\mathbb{O}}$	kg m^{-3}	1000	1.2
$S_{\mathbb{W}dr}$	$S_{\mathbb{O}im}$		0.13	0.21
η_2	η_4		6	4
α	β		0.42	1.6
P_a	P_b	Pa	2700	3
γ	δ		2.4	2.9
P_2^*	P_4^*	Pa	11,000	3000
R_{11}	R_{33}	kg m^{-3} s^{-1}	3.83×10^6	6.99×10^4
R_{22}	R_{44}	kg m^{-3} s^{-1}	10^{16}	10^{16}
R_{ij}, $i \neq j$		kg m^{-3} s^{-1}	0	

[a]Note that ϵ_M is a mathematical regularization parameter, i.e., the limit $\epsilon_M \to 0$ is implicit and it has been tested that the numerical results do not change in this limit.

P_b, P_2^*, P_4^* are the constitutive parameters. The parameters α, β, P_a, P_b are associated with capillary potentials and $\gamma, \delta, P_2^*, P_4^*$ with the energy stored in the interface between the nonpercolating phases and the surrounding percolating phases of the other fluid [*Hilfer*, 2006b]. A generalized mobility matrix is denoted by Λ with the coefficients

$$\Lambda_{ij} = \phi^2 S_i S_j [\tilde{R}^{-1}]_{ij}, \tag{5}$$

where $[\tilde{R}^{-1}]_{ij}$ denote the components of the inverse of the viscous coupling parameter matrix. A comparison with the classical two-phase Darcy equations yields that $\tilde{R}_{11} \approx \mu_{\mathbb{W}}/k$ and $\tilde{R}_{33} \approx \mu_{\mathbb{O}}/k$, where k denotes the permeability of the porous medium. The system of equations is closed with the volume conservation for incompressible fluids and incompressible porous media

$$S_1 + S_2 + S_3 + S_4 = 1 \tag{6}$$

plus a special form of the general selfconsistent closure condition [*Hilfer and Doster*, 2009; *Doster et al*., 2010]

$$P_3 = P_1 + \frac{1}{2}\left(P_a S_1^{-\alpha} - P_b S_3^{-\beta} + \gamma P_2^* S_2^{\gamma-1} - \delta P_4^* S_4^{\delta-1}\right) \tag{7}$$

for the pressures of the percolating phases.

4. Simulation Setup

[10] In this section, we discuss how the experiment is represented mathematically. The four mass balance equations (1) are solved numerically. First, equations (6) and (7) are used to eliminate S_4 and P_3. The primary variables are S_1, S_2, S_3, and P_1. The mass balances are discretized in space by cell centered finite volumes with upwind fluxes. They are discretized in time with a first-order implicit fully coupled scheme. The corresponding system of nonlinear equations is solved with the Newton-Raphson method. The whole scheme is implemented in Matlab. The simulation is run with a resolution of one cell per centimeter, i.e., with $N = 72$ collocation points. Details of the algorithm are given elsewhere [*Doster*, 2011].

[11] Dirichlet boundary conditions for the pressure P_1 of the percolating water phase are imposed at the lower boundary ($x = 0$ m), where pressure is determined by the water reservoir. Dirichlet boundary conditions for the atmospheric pressure P_3 of the percolating air phase are chosen at the upper boundary ($x = 0.72$ m) of the column. All the other boundaries are impermeable so that the flux across them must vanish.

[12] The initial conditions are $S_1(x,0) = 0.997, S_2(x,0) = 0.001, S_3(x,0) = 0.001$, and $S_4(x,0) = 0.001$ for all $x \in [0\,\text{cm}, 72\,\text{cm}]$. Initial conditions for the pressures are not required because of the implicit formulation. Before the protocol for the pressure is started, the system is given 1 day under hydrostatic water pressure conditions to equilibrate.

[13] The parameters for the simulation are given in Table 1. They were obtained by fitting the primary drainage curve of the capillary pressure-saturation relationship obtained in the residual decoupling approximation [*Hilfer*, 2006b] to the primary drainage curve of van Genuchten parameterization that *Lenhard et al*. [1991] obtained by a fit to data of the first drainage process in the experiment. The van Genuchten parameters in *Lenhard et al*. [1991] are $\alpha^{dr} = 4.28 \times 10^{-4}\text{Pa}^{-1}$, $\alpha^{im} = 8.56 \times 10^{-4}\text{Pa}^{-1}$, $n^{dr} = 5.52$, $n^{im} = 5.52$, $m^{dr} = 0.82$, $m^{im} = 0.82$, $S_{wi} = 0.17$, and $S_{nr} = 0.25$. The resulting capillary pressure curves are compared in Figure 2. The viscous resistance coefficients were obtained through $R_{11} \approx \mu_{\mathbb{W}}/k$ and $R_{33} \approx \mu_{\mathbb{O}}/k$, where $k = 33.7^{-12}\,\text{m}^2$ was again taken from *Lenhard et al*. [1991]. The viscous resistance coefficients for the nonpercolating phases are assumed to be much larger than those for the percolating phases $R_{22}, R_{44} \gg R_{11}, R_{33}$. For the time scale of the experiment, the results do not depend on the numerical values of the resistance coefficients given in Table 1 [*Doster*, 2011].

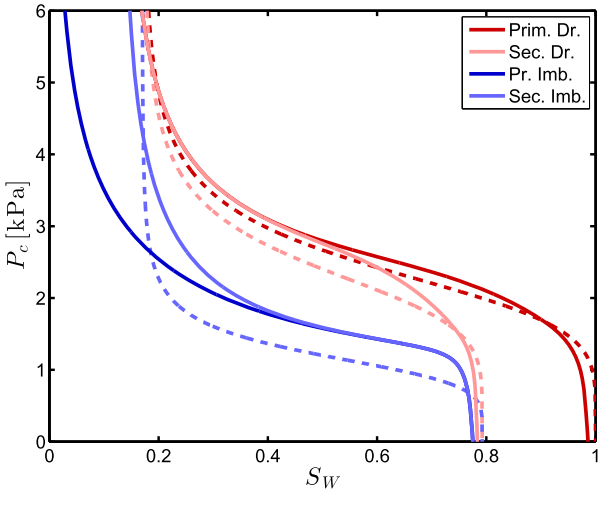

Figure 2. Illustration of the capillary pressure-saturation relationship in the residual decoupling approximation of our theory for the parameters given in Table 1 (solid lines) for primary and secondary drainage and imbibitions, respectively. Also shown are the primary and secondary drainage and the secondary imbibition curve of the hysteresis model used in *Lenhard et al*. [1991] (dashed curves).

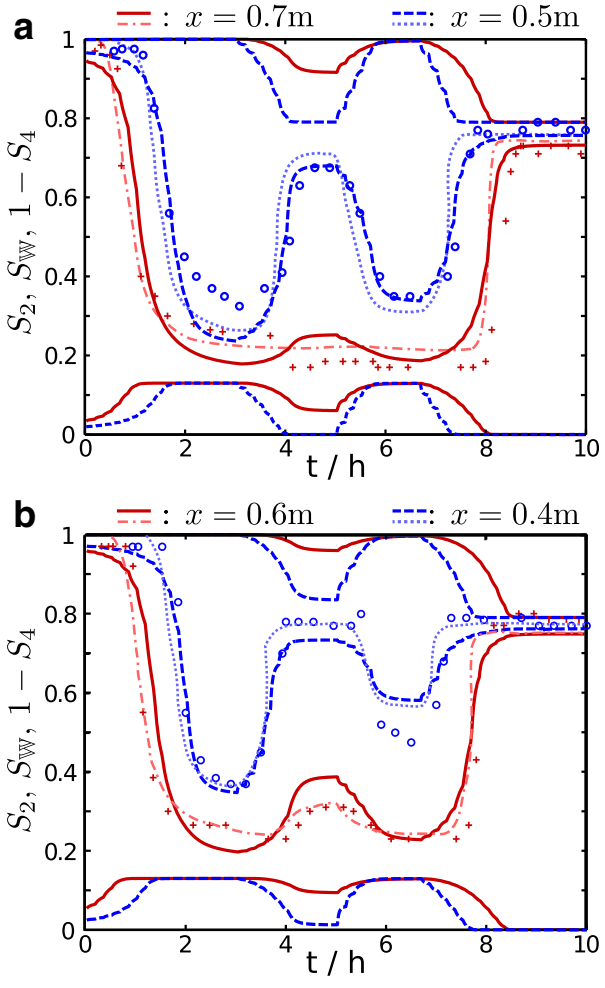

Figure 3. Comparison of the water saturation $S\mathbb{W}(x,t)$ at x=0.4 m and x=0.5 m (blue curves), and x=0.6 m and x=0.7 m (red curves) from simulation and experiment. Solid and dashed curves show our simulations and dotted and dash-dotted curves the simulation of *Lenhard et al.* [1991]. Experimental data are illustrated by red pluses (x=0.7 m and x=0.6 m) and blue circles (x=0.5 m and x=0.4 m). Also shown are the results for $S_2(x,t)$ (the first dashed and solid curves from the bottom of each graph) and $1-S_4(x,t)$ (the first dashed and solid curves from the top of each graph).

5. Results

[14] The results of the simulations are compared with the experimental data and the most sophisticated model of *Lenhard et al.* [1991] (previously developed in *Parker and Lenhard* [1987]; *Lenhard and Parker* [1987]) in Figures 3 and 4. Figure 3 shows the computed time evolution of $S_{\mathbb{W}}(x,t), S_2(x,t), S_4(x,t)$ at x=0.4 m, x=0.5 m, x=0.6 m, and x=0.7 m as continuous and dashed lines. The experimental data for $S_{\mathbb{W}}$ are shown as plus signs and circles and the simulation results with the most sophisticated model of *Lenhard et al.* [1991] are represented by dash-dotted and dotted curves. There is a good qualitative agreement at all four positions.

[15] During the first 2 h of the experiment, the saturation decreases because of the lowered pressure in the water reservoir. The instants at which the capillary fringe passes the measurement points agree at all four points between simulation and measurement. The decrease in water saturation induces a production of nonpercolating water. The corresponding decrease in nonpercolating air is not visible in the graph because of the small amount of initial nonpercolating air. The pressure does not change between t=2h and t=3.5h. Hence, the rate of saturation change decreases and saturation reaches an almost stationary value. The calculated water saturations of that plateau are slightly smaller than the experimental ones. Measured and predicted values during the first increase of the reservoir pressure at around $t \approx$ 4h show good agreement excluding x=0.70 m. In contrast to the simulated saturation, the measured saturation decreases at x=0.70 m after an increase of the pressure at the lower boundary. This surprising effect was not discussed in the experimental work [*Lenhard et al.*, 1991] and the lack of error bars makes an interpretation difficult

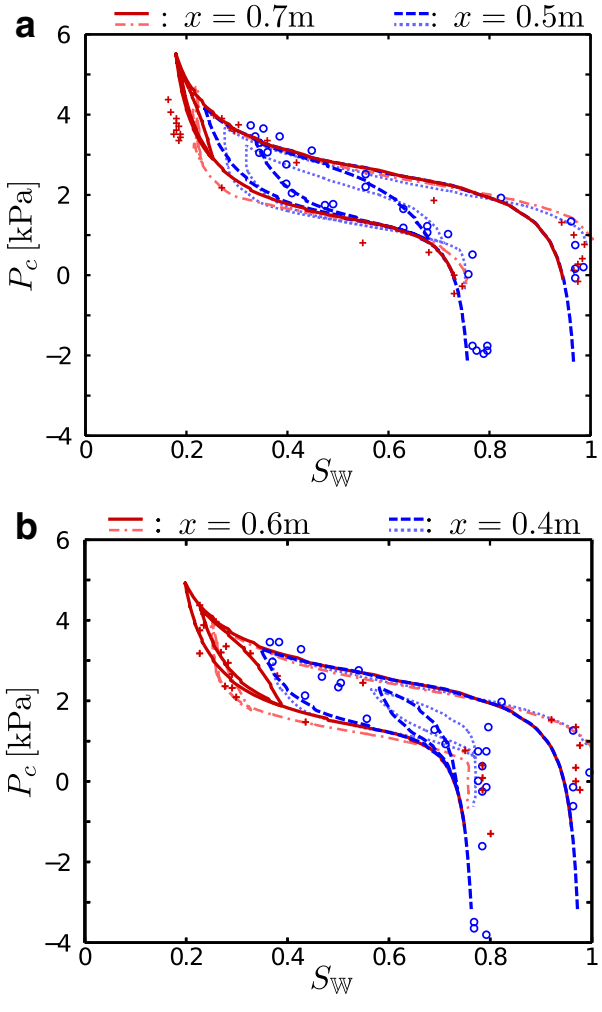

Figure 4. Comparison of measured and simulated capillary pressure-saturation relationship $Pc(S_{\mathbb{W}}(x,t))$ at x=0.4 m, x=0.5 m (blue curves) and x=0.6 m, x=0.7 m (red curves). Solid and dashed curves show our simulations and dotted and dash-dotted curves the simulation of *Lenhard et al.* [1991]. Experimental data are illustrated by red pluses (x=0.7 m and x=0.6 m) and blue circles (x=0.5 m and x=0.4 m).

Table A1. List of Unknowns Needed at a Given Time Instant t to Compute the Future Time Evolution for the Mathematical Model in this Paper as Compared to the Mathematical Model of *Lenhard et al*. [1991][a]

This theory	*Lenhard et al*. [1991]
$S_{\mathbb{W}}(x_i,t)$	$S_w(x_i,t)$
$S_2(x_i,t)$	–
$S_4(x_i,t)$	–
$P_3(x_i,t)$	$h_{nw}(x_i,t)$
–	$^{\Delta}\overline{S}_{w1}(x_i,t_1)=1$
–	$^{\Delta}h_{nw1}(x_i,t_1)=0$
–	$^{\Delta}\overline{S}_{w2}(x_i,t_2(x_i))$
–	$^{\Delta}h_{nw2}(x_i,t_2(x_i))$
...	...
–	$^{\Delta}\overline{S}_{wl(x_i)-1}(x_i,t_{l(x_i)-1}(x_i))$
–	$^{\Delta}h_{nwl(x_i)-1}(x_i,t_{l(x_i)-1}(x_i))$
–	$^{\Delta}\overline{S}_{wl(x_i)}(x_i,t_{l(x_i)}(x_i))$
–	$^{\Delta}h_{nwl(x_i)}(x_i,t_{l(x_i)}(x_i))$

[a]Quantities corresponding to each other appear in the same row. The arguments x_i denote N discretized positions, i.e., collocation points $i=1,...,N$ of the numerical simulation. The notation of in the right column follows *Lenhard et al*. [1991], the notation in the left column is that of this paper. The time instants $t_j(x_i), j=1,...,l(x_i)$ are the time instant of the jth reversal at position x_i. The number $l(x_i)$ of reversals (nested scanning curves) depends on position x_i.

(similar experiments *Lenhard et al*. [1993] by the same authors suggest error bars of order $\Delta S_{\mathbb{W}} \approx 0.1$). The increase of water saturation induces a decrease of nonpercolating water and a production nonpercolating air.

[16] The subsequent evolution of the saturation shows qualitatively similar phenomena upon changing the pressure. Note, that the spatiotemporal evolution of the saturation requires an infinite number of scanning curves in traditional hysteresis modeling, i.e., when the process changes between drainage and imbibition as a function of time and position. Here in our model, a single set of parameters is sufficient, and there is no need to know scanning curves beforehand. At the end of the experiment, water is almost completely connected at all four measurement positions, while most of the air is disconnected and trapped. The trapped air prevents the complete filling of the column with water and indicates the irreversibility of the process.

[17] Figure 4 illustrates the hysteretic drainage and imbibition processes in the $P\mathrm{c}-S_{\mathbb{W}}$ plane. It shows $P\mathrm{c}(S_{\mathbb{W}})$ obtained by eliminating x and t from the measurements of $-P_1(x,t)$ and $S_{\mathbb{W}}(x,t)$ at $x=0.4$ m, $x=0.5$ m, $x=0.6$ m, and $x=0.7$ m. The lines of the simulations indicate the time evolution which is compared to the time discrete observations in the experiment. Experimental and simulated data agree qualitatively. The values at $S_{\mathbb{W}} \approx 0.99$ corresponds to the minimum in the pressure protocol of the water reservoir (see Figure 1) at the start of the experiment. The decrease in water saturation induces an increase in P_c during the primary drainage and the curves of all four positions coincide with the experimental data. The point with the lowest saturation of each primary drainage branch corresponds to the instant when the pressure in the water reservoir is increased again. The deviations between simulation and experiment at $x=0.7$ m and $x=0.5$ m originate from the mismatched saturations (see Figure 3). The following imbibition discloses the hysteretic nature of the process as the curves at the four different positions follow different scanning curves. Also the subsequent drainage yields different drainage scanning curves. This branch of the curve is difficult to identify in the experimental data at $x=0.7$ m and $x=0.6$ m but matches well at the other two locations. The final imbibition yields saturation $S_{\mathbb{W}} \approx 0.8$ and the curves at all four positions almost coincide again.

[18] The figures show that the quality of our results is comparable to the most sophisticated model used in *Lenhard et al*. [1991]. However, in our theory, the hysteresis in saturation profiles is due to the natural assumption that breakup and coalescence rates are proportional to the rate and direction of saturation change, whereas in their models, the hysteresis is nonlocal in time and inserted directly by hand into the constitutive functions. The good quality of the results is surprising because it is evident that some of our assumptions such as the incompressibility of air and the incompressible porous medium are questionable. We remark also, that the lack of error bars for the experimental data makes an interpretation difficult.

6. Conclusions

[19] In summary, we presented a comparison of experimental observations with theoretical predictions for a theory of two-phase flow in porous media based on the hydraulic differences between percolating and nonpercolating fluid parts. It was shown that taking into account these differences renders the modeling of a multistep outflow capillary pressure-saturation relationship measurement possible with one single set of parameters. In contrast to most of the hysteretic extension of the standard theory for two-phase flow in porous media, the underlying theory has a physical foundation. We, therefore, conclude that percolation of fluid phases may be the physical reason for hysteresis between drainage and imbibition during immiscible displacement.

Appendix A

[20] This appendix considers some computational aspects of our theory to aid readers simulating experiments with hysteresis. It clarifies fundamental differences (locality versus nonlocality) between the theory presented here and a traditional hysteresis model. The natural assumption in equation (2), that breakup or coalescence of ganglia is proportional to the rate and direction of saturation changes, is neither equivalent nor related to the traditional hysteretic extensions of capillary pressure or relative permeabilities.

[21] The origin of hysteresis in the present theory [see *Hilfer*, 2006b, 2006c] differs fundamentally from traditional hysteresis models such as the model utilized in *Lenhard et al*. [1991]. Traditional hysteresis models require to store for each location inside the sample the pressure and saturation history (i.e., the reversal points, where the process switches between drainage and imbibition). In our theory, such pressure and saturation histories are not needed. Instead, contrary to traditional hysteresis models, our theory allows to compute the future state of the porous medium, given only the knowledge of its present state. In other words, while traditional hysteresis models are nonlocal in time (and thus require to memorize the systems history), our theory is local in time.

[22] In practical computations, the locality of our theory translates into reduced storage requirements and a more straightforward implementation. Table A1 below lists the fields (i.e., the position and time-dependent quantities) necessary to compute the future time evolution of the system.

[23] Both approaches need a pressure and saturation field at the present time instant t. Our theory needs in addition the unknowns S_2, S_4 to completely specify the present state of the system. This amounts to two additional state variables at each collocation point. Traditional hysteresis models need in addition $2l(x_i)$ historic values, one for pressure and one for saturation, at each collocation point x_i. The number $l(x_i)$ is the number of time instants $t_j(x_i)$, $j=1, ..., l(x_i)$ at which reversals occur at position $x_i, i=1, ..., N$. A reversal is a switching between drainage and imbibition at the collocation point x_i. The number $l(x_i)$ depends on the nesting or not of scanning curves. The number $l(x_i)$ and the time instants $t_j(x_i)$ are not known in advance. In *Lenhard et al*. [1991], it is assumed ad hoc that nested loops do not occur and that the last two reversals are sufficient to avoid pumping effects. This uncontrolled approximation might fail for experiments with cyclic pressure changes where nested scanning loops are expected to occur locally. In the general case, *Lenhard et al*. [1991] expect that the last four or five reversals are sufficient.

[24] Finally, it may be of interest for practical computations that the model of *Lenhard et al*. [1991] postulates explicitly and implicitly numerous functional relations between the variables and unknowns characterizing the state of the system. Examples are not only the capillary pressure-saturation relationship or the relative permeability-saturation relationship, but also the functional relations between the various effective, apparent, entrapped, and historic saturations and pressures $\overline{S}_w, \overline{\overline{S}}_w$, $h_{nw}, \overline{S}_{nt}, \overline{S}_{nr}, {}^{\Delta}h_{nwj}$, and ${}^{\Delta}\overline{S}_{wj}$ appearing in *Lenhard et al*. [1991]. The functional forms for these relationships are postulated purely theoretically and have, apparently, been tested by inverse fitting but not yet by a direct experimental test. The large number of such functional relations and the freedom to parameterize them results in so many possible fit parameters for the model of *Lenhard et al*. [1991] that a meaningful comparison to other approaches based on the number of free fit parameters becomes difficult.

[25] **Acknowledgments.** The authors gratefully acknowledge financial support from the Deutsche Forschungsgemeinschaft and thank Andreas Lauser for technical assistance.

References

Bear, J. (1972), *Dynamics of Fluids in Porous Media*, Dover, New York.

Buckingham, E. (1907), *Studies on the Movement of Soil Moisture*, vol. 38, Bull., *U.S. Dep. of Agric., Bur. of Soils*, Washington, D.C., US, pp. 1–61.

Doster, F. (2011), Die bedeutung perkolierender und nichtperkolierender phasen bei mehrphasenströmungen in porösen medien auf laborskala, PhD thesis, Univ. Stuttgart, Stuttgart, Germany.

Doster, F., and R. Hilfer (2011), Generalized Buckley-Leverett theory for two phase flow in porous media, *New J. Phys.*, *13*, 123030.

Doster, F., P. A. Zegeling, and R. Hilfer (2010), Numerical solutions of a generalized theory for macroscopic capillarity, *Phys. Rev. E*, *81*(3), 036307, doi:10.1103/PhysRevE.81.036307.

Doster, F., O. Hönig, and R. Hilfer (2012), Horizontal flow and capillarity-driven redistribution in porous media, *Phys. Rev. E*, *86*(1), 016317.

Gerhard, J., and B. Kueper (2003), Relative permeability characteristics necessary for simulating DNAPL infiltration, redistribution, and immobilization in saturated porous media, *Water Resour. Res.*, *39*(8), 1213, doi:10.1029/2002WR001490.

Hilfer, R. (2006a), Capillary pressure, hysteresis and residual saturation in porous media, *Physica A*, *359*, 119–128.

Hilfer, R. (2006b), Macroscopic capillarity and hysteresis for flow in porous media, *Phys. Rev. E*, *73*, 016307.

Hilfer, R. (2006c), Macroscopic capillarity without a constitutive capillary pressure function, *Physica A*, *371*, 209–225.

Hilfer, R., and F. Doster (2009), Percolation as a basic concept for macroscopic capillarity, *Transp. Porous Media*, *82*(3), 507–519, doi:10.1007/s11242-009-9395-0.

Hönig, O., F. Doster, and R. Hilfer (2013), Traveling wave solutions in a generalized theory for macroscopic capillarity, *Transp. Porous Media*, *99*, 467–491, doi:10.1007/s11242-013-0196-0.

Lake, L. W. (1989), *Enhanced Oil Recovery*, Prentice Hall, Upper Saddle River, N. J.

Land, C. S. (1968), Calculation of imbibition relative permeability for two- and three phase flow from rock properties, *Trans. Am. Inst. Min. Metall. Pet. Eng.*, *243*, 149–156.

Lenhard, R., J. Parker, and J. Kaluarachchi (1991), Comparing simulated and experimental hysteretic two-phase transient fluid flow phenomena, *Water Resour. Res.*, *27*, 2113–2124.

Lenhard, R., T. Johnson, and J. Parker (1993), Experimental observations of nonaqueous-phase liquid subsurface movement, *J. Contam. Hydrol.*, *12*(1–2), 79–101, doi:10.1016/0169-7722(93)90016-L.

Lenhard, R. J., and J. C. Parker (1987), A model for hysteretic constitutive relations governing multiphase flow: 2. Permeability-saturation relations, *Water Resour. Res.*, *23*, 2197–2206.

Mualem, Y. (1973), Modified approach to capillary hysteresis based on a similarity hypothesis, *Water Resour. Res.*, *9*, 1324–1331.

Mualem, Y. (1974), A conceptual model of hysteresis, *Water Resour. Res.*, *10*, 514–520.

Muskat, M., and M. Meres (1936), The flow of heterogeneous fluids through porous media, *Physics*, *7*, 346.

Parker, J. (1989), Multiphase flow and transport in porous-media, *Rev. Geophys.*, *27*, 311–328.

Parker, J. C., and R. J. Lenhard (1987), A model for hysteretic constitutive relations governing multiphase flow: 1. Saturation pressure relations, *Water Resour. Res.*, *23*, 2187–2196.

Richards, L. A. (1931), Capillary conduction of liquids through porous medium, *Physics*, *1*, 318–333.

Stauffer, F. (1978), Time dependence of the relations between capillary pressure, water content and conductivity during drainage of porous media. IAHR Symp. on Scale Effects in Porous Media. Thessaloniki, Greece. 29 Aug.–1 Sept. 1978. International Association for Hydro-Environmental Engineering and Research (IAHR), Madrid, Spain.

Wei, C., and M. Dewoolkar (2006), Formulation of capillary hysteresis with internal state variables, *Water Resour. Res.*, *42*, W07405, doi:10.1029/2005WR004594.

Wyckoff, R. D., and H. G. Botset (1936), The flow of gas-liquid mixtures through unconsolidated sands, *Physics*, *7*(9), 325–345, doi:10.1063/1.1745402.